An efficient numerical algorithm for computing densely distributed positive interior transmission eigenvalues

Tiexiang Li

Department of Mathematics, Southeast University, Nanjing 211189, People's Republic of China.

E-mail: txli@seu.edu.cn

Tsung-Ming Huang

Department of Mathematics, National Taiwan Normal University, Taipei 116, Taiwan.

E-mail: min@ntnu.edu.tw

Wen-Wei Lin

Department of Applied Mathematics, National Chiao Tung University, Hsinchu 300, Taiwan.

E-mail: wwlin@math.nctu.edu.tw

Jenn-Nan Wang

Institute of Applied Mathematical Sciences, NCTS, National Taiwan University, Taipei, 106, Taiwan.

E-mail: jnwang@math.ntu.edu.tw

Abstract. We propose an efficient eigensolver for computing densely distributed spectrum of the two-dimensional transmission eigenvalue problem (TEP) which is derived from Maxwell's equations with Tellegen media and the transverse magnetic mode. The discretized governing equations by the standard piecewise linear finite element method give rise to a large-scale quadratic eigenvalue problem (QEP). Our numerical simulation shows that half of the positive eigenvalues of the QEP are densely distributed in some interval near the origin. The quadratic Jacobi-Davidson method with a so-called non-equivalence deflation technique is proposed to compute the dense spectrum of the QEP. Extensive numerical simulations show that our proposed method makes the convergence efficiently even it needs to compute more than 5000 desired eigenpairs. Numerical results also illustrate that the computed eigenvalue curves can be approximated by the nonlinear functions which can be applied to estimate the denseness of the eigenvalues for the TEP.

Keywords: Two-dimensional transmission eigenvalue problem, Tellegen model, transverse magnetic mode, quadratic Jacobi-Davidson method, non-equivalence deflation

1. Introduction

The transmission eigenvalue problems (TEP) have recently received a great deal of attention in the area of the inverse scattering which is essential in the study of direct/inverse scattering problems for nonabsorbing inhomogeneous media [3, 4, 5, 6, 8, 10, 11, 20, 27]. The existence of transmission eigenvalues is closely related to the validity of some reconstruction methods for the inverse scattering problems in an inhomogeneous medium such as the linear sampling method [1, 7] and the factorization method [21]. On the other hand, it has been shown that transmission eigenvalues can be estimated by using the far-field data [2] or the near-field data (Cauchy data) [30]. In fact, both Dirichlet eigenvalues and transmission eigenvalues carry the information of the scatterer and can be estimated by either the far-field or the near-field data. For example, the Herglotz wave function [9] is applied at the first Dirichlet eigenvalue to reconstruct the shape of the sound-soft scatterer. The eigenvalue method using multiple frequency near-field data (EM^{2}F) [32] is proposed to detect Dirichlet or transmission eigenvalues and to reconstruct the support of the scatterer by determining the indicator function. In addition, the EM^{2}F can be used to distinguish between the sound-soft obstacle and nonabsorbing inhomogeneous medium. For further study in the theories and applications of TEP, we refer to [6] and the references therein for further details.

In this paper, we consider the scattering of acoustic waves by an inhomogeneous medium which occupies a bounded and simply connected domain $D \subseteq \mathbb{R}^2$. The related so-called TEP is to find $\lambda > 0$ and nontrivial functions $u, v \in L^2(D)$ with $u - v \in H_0^2(D) = \{ w \in H^2 | \, w = 0, \frac{\partial w}{\partial \nu} = 0 \text{ on } \partial D \}$ satisfying

$$\Delta u + \lambda \varepsilon(x, y) u = 0, \quad \text{in } D, \tag{1a}$$

$$\Delta v + \lambda v = 0, \quad \text{in } D, \tag{1b}$$

where ν is the outer unit normal to the smooth boundary ∂D and $\varepsilon(x, y)$ is the index of refraction. Any positive λ such that (1) has nontrivial solutions u and v is called an interior transmission eigenvalue. Note that $u - v \in H_0^2(D)$ is equivalent to

$$u = v \quad \text{on} \quad \partial D, \tag{2a}$$

$$\frac{\partial u}{\partial \nu} = \frac{\partial v}{\partial \nu} \quad \text{on} \quad \partial D. \tag{2b}$$

Equation (1a) can be regarded as the reduced Maxwell equations with transverse magnetic (TM) modes. In this paper, we will consider the case where the parameter $\varepsilon(x, y)$ are chosen sufficiently large. For the standard Maxwell equations, ε corresponds to the electric permittivity which is written as the product of the relative permittivity and the free space permittivity. In practice, ε can not be taken as large as we wish. Therefore, in this paper, we will derive (1a) from Maxwell's equations with Tellegen media (non-reciprocal and non-chiral). It turns out for this case ε is the sum of the electric permittivity and the square of Tellegen parameter. By choosing large Tellegen parameter, we can enlarge the parameter ε as well.

There are several theoretical results regarding the existence of interior transmission eigenvalues [4, 5, 20, 27]. Several numerical algorithms for computing the transmission eigenvalues were proposed recently. Three finite element methods (FEMs) and a coupled boundary element method were proposed for solving the two-dimensional (2D)/three-dimensional (3D) interior transmission eigenvalue problems in [10, 12, 33], and, furthermore, in a recently published book [34] for details. In view of the existence theory of the transmission eigenvalues based on the fourth order reformulation in [5], two iterative methods together with convergence analysis were studied in [31]. In [18], a mixed FEM for 2D TEP was proposed, which leads to a non-Hermitian quadratic eigenvaluue problem (QEP) and then was solved by an adaptive Arnoldi method. On the other hand, the multilevel correction method was used to reduce the solution of TEP into a series of solutions to some linear boundary value problems which could be solved by the multigrid method [19].

In many cases with general inhomogeneous medium, the desired positive transmission eigenvalues are surrounded by complex ones. Based on complex-valued contour integrals and the boundary integral equation, an accurate numerical method for computing interior transmission eigenvalues for many obstacles (different from spheres) in 3D acoustic scattering was presented in [22]. However, only constant index of refraction and smooth domains were treated there. The algorithm used in [22] was later extended to the electromagnetic case in [23, 24]. The QEP above can be rewritten as a particular parametrized symmetric definite generalized eigenvalue problem (GEP). For such GEP, the eigenvalue curves can be arranged in a monotonic order so that the desired curves are sequentially located by a new secant-type iteration (see [25] for 2D TEP and [13] for 3D TEP, respectively).

In this paper, we focus on the 2D TEP with complex media and make the following contributions.

- We derive the 2D TEP (1) with $\varepsilon(x, y) = \tilde{\varepsilon}(x, y) + \gamma^2$ from the Maxwell's equation with non-reciprocal, non-chiral media and the transverse magnetic mode (TM). Here $\tilde{\varepsilon}(x, y)$ is the electric permittivity and γ is the Tellegen parameter.
- Discretized (1) by the standard piecewise linear finite element method [10] results in a GEP. The GEP is then reduced to a QEP by deflating all nonphysical zeros. Our numerical simulations indicate that half of the positive eigenvalues of the QEP are densely distributed in some interval.
- We adapt the quadratic Jacobi-Davidson (QJD) method with partial locking technique for computing a large number of desired eigenpairs of the QEP. In order to accelerate convergence, we also develop a so-called partial non-equivalence deflation technique combined with QJD to deflate the part of computed eigenvalues to infinity while keeping the other eigenvalues unchanged. Numerical results demonstrate that the new partial deflation technique makes the convergence efficiently for computing 5000 desired eigenpairs.
- Furthermore, we modify QJD with partial deflation technique so that it can be

applied to compute all the eigenvalues in a given interval. Therefore, we separate the densely distributed eigenvalues of the TEP into several subintervals and compute the desired eigenpairs simultaneously by the modified method. Numerical results show that this modified method can be applied to compute more than 10000 target eigenpairs in our model.

- According to the computed eigenvalues, we find that the logarithms of the eigenvalue curves vs $\log_{10}(\varepsilon(x,y))$ for the TEP (1) are approximated by straight lines with almost the same negative slope. Therefore, we can estimate the distribution of the eigenvalues for given $\varepsilon(x,y)$ from these parallel straight lines.

This paper is organized as follows. Section 2 is devoted to derive a 2D TEP with TM mode in non-reciprocal, non-chiral media. A corresponding discretization TEP and its spectral analysis are given in Section 3. In Section 4, we develop a non-equivalence low-rank deflation which can be used to accelerate convergence of QJD for computing the desired positive eigenvalues. A practical QJD algorithm combined with non-equivalence deflation and numerical results are presented in Sections 5 and 6, respectively. Finally, a concluding remark is given in Section 7.

2. Description of the governing equation

We consider Maxwell's equations in complex media [35]:

$$\nabla \times E = \mathrm{i}\omega\left(\mu H + \zeta E\right), \tag{3a}$$

$$\nabla \times H = -\mathrm{i}\omega\left(\tilde{\varepsilon} E + \xi H\right), \tag{3b}$$

where E and H are the electronic field and magnetic field, respectively, ω represents the frequency, $\tilde{\varepsilon}$ and μ are the permittivity and the permeability, respectively, ξ and ζ are 3-by-3 magnetoelectric parameter matrices in various forms for describing different types of materials (see [28, p.26] and [35, p.44]). In this paper, we assume $\mu = 1$ and all other parameters are functions of x, y. For this situation, we study the TM mode for (3), i.e.,

$$E = \begin{bmatrix} 0 & 0 & E_3(x,y) \end{bmatrix}^\top, \quad H = \begin{bmatrix} H_1(x,y) & H_2(x,y) & 0 \end{bmatrix}^\top. \tag{4}$$

Let

$$\zeta = \begin{bmatrix} 0 & 0 & \zeta_1 \\ 0 & 0 & \zeta_2 \\ -\zeta_1 & -\zeta_2 & 0 \end{bmatrix}, \quad \xi = \begin{bmatrix} 0 & 0 & \xi_1 \\ 0 & 0 & \xi_2 \\ -\xi_1 & -\xi_2 & 0 \end{bmatrix}. \tag{5}$$

Then, Eqs. (3a) implies that

$$\begin{bmatrix} \partial_y E_3 \\ -\partial_x E_3 \\ 0 \end{bmatrix} = \mathrm{i}\omega \left(\begin{bmatrix} H_1 \\ H_2 \\ 0 \end{bmatrix} + \begin{bmatrix} \zeta_1 E_3 \\ \zeta_2 E_3 \\ 0 \end{bmatrix} \right). \tag{6}$$

Substituting (6) into (3b) yields

$$
\begin{aligned}
&(\mathrm{i}\omega)^{-1}\begin{bmatrix} 0 \\ 0 \\ -\left(\frac{\partial^2}{\partial x^2}+\frac{\partial^2}{\partial y^2}\right)E_3 \end{bmatrix} - \begin{bmatrix} 0 \\ 0 \\ \frac{\partial}{\partial x}\left(\zeta_2 E_3\right) - \frac{\partial}{\partial y}\left(\zeta_1 E_3\right) \end{bmatrix} \\
&= -\mathrm{i}\omega\left(\tilde{\varepsilon}\begin{bmatrix} 0 \\ 0 \\ E_3 \end{bmatrix} - \begin{bmatrix} 0 \\ 0 \\ \xi_1 H_1 + \xi_2 H_2 \end{bmatrix}\right),
\end{aligned}
$$

which implies that

$$
\begin{aligned}
&-\Delta E_3 \\
&= \omega^2\left[\tilde{\varepsilon}E_3 - \xi_1\left((\mathrm{i}\omega)^{-1}\frac{\partial}{\partial y}E_3 - \zeta_1 E_3\right) + \xi_2\left((\mathrm{i}\omega)^{-1}\frac{\partial}{\partial x}E_3 + \zeta_2 E_3\right)\right] \\
&\quad + \mathrm{i}\omega\left[\frac{\partial}{\partial x}\left(\zeta_2 E_3\right) - \frac{\partial}{\partial y}\left(\zeta_1 E_3\right)\right] \\
&= \omega^2\left(\tilde{\varepsilon} + \xi_1\zeta_1 + \xi_2\zeta_2\right)E_3 + \mathrm{i}\omega\left[\frac{\partial}{\partial x}\left(\zeta_2 E_3\right) - \frac{\partial}{\partial y}\left(\zeta_1 E_3\right) + \xi_1\frac{\partial}{\partial y}E_3 - \xi_2\frac{\partial}{\partial x}E_3\right].
\end{aligned}
$$

If we choose $\zeta_1 = \xi_1 = \gamma_1$ and $\zeta_2 = \xi_2 = \gamma_2$, where γ_1, γ_2 are real constants, then we have

$$
-\Delta E_3 = \omega^2\left[\tilde{\varepsilon} + \left(\gamma_1^2 + \gamma_2^2\right)\right]E_3 \equiv \omega^2\varepsilon(x,y)E_3 \tag{7}
$$

with

$$
\varepsilon(x,y) = \tilde{\varepsilon}(x,y) + \gamma_1^2 + \gamma_2^2. \tag{8}
$$

Maxwell's equations with real parameters $\zeta = \xi$ are called Tellegen model.

We now discuss the boundary conditions. Recall that ν is the outer unit normal to ∂D. Then it is readily seen that

$$
E \times \nu = \begin{bmatrix} 0 \\ 0 \\ E_3 \end{bmatrix} \times \begin{bmatrix} \nu_1 \\ \nu_2 \\ 0 \end{bmatrix} = \begin{bmatrix} -\nu_2 E_3 \\ \nu_1 E_3 \\ 0 \end{bmatrix}
$$

and

$$
(\nabla \times E) \times \nu = \begin{bmatrix} \frac{\partial}{\partial y}E_3 \\ -\frac{\partial}{\partial x}E_3 \\ 0 \end{bmatrix} \times \begin{bmatrix} \nu_1 \\ \nu_2 \\ 0 \end{bmatrix} = \begin{bmatrix} \frac{\partial E_3}{\partial y}\nu_2 + \frac{\partial E_3}{\partial x}\nu_1 \\ 0 \\ 0 \end{bmatrix} = \begin{bmatrix} \frac{\partial E_3}{\partial \nu} \\ 0 \\ 0 \end{bmatrix}.
$$

In other words, boundary conditions $E \times \nu|_{\partial D}$ and $(\nabla \times E) \times \nu|_{\partial D}$ are equivalent to

$$
E_3|_{\partial D} \quad \text{and} \quad \frac{\partial E_3}{\partial \nu}|_{\partial D}.
$$

We then arrive at the TEP for (1a)-(1b) and (2a)-(2b) with $\varepsilon(x,y)$ given in (8).

3. Discretization of TEP and its spectral analysis

We briefly review the discretization of the TEP (1) based on the standard piecewise linear FEM (see [10] for details). Let

$$\begin{aligned} S_h &= \text{The space of continuous piecewise linear functions on } D, \\ S_h^I &= \text{The subspace of functions in } S_h \text{ with vanishing DoF on } \partial D, \\ S_h^B &= \text{The subspace of functions in } S_h \text{ with vanishing DoF in } D. \end{aligned}$$

Here DoF stands for degrees of freedom. Let $\{\phi_i\}_{i=1}^n$ and $\{\psi_i\}_{i=1}^m$ denote standard nodal bases for the finite element spaces of S_h^I and S_h^B, respectively, then

$$u = u_h^I + u_h^B = \sum_{i=1}^n u_i \phi_i + \sum_{i=1}^m w_i \psi_i, \tag{9a}$$

$$v = v_h^I + v_h^B = \sum_{i=1}^n v_i \phi_i + \sum_{i=1}^m w_i \psi_i. \tag{9b}$$

Applying the standard piecewise linear finite element method to (1a) and using integration by parts, we get

$$\begin{aligned} &\sum_{i=1}^n u_i \left(\nabla \phi_i, \nabla \phi_j\right) + \sum_{j=1}^m w_i \left(\nabla \psi_i, \nabla \phi_j\right) \\ &= \omega^2 \left(\sum_{i=1}^n u_i \left(\varepsilon \phi_i, \phi_j\right) + \sum_{i=1}^m w_i \left(\varepsilon \psi_i, \phi_j\right) \right). \end{aligned} \tag{10}$$

Similarly, applying the standard piecewise linear finite element method to (1b), we have

$$\sum_{i=1}^n v_i \left(\nabla \phi_i, \nabla \phi_j\right) + \sum_{j=1}^m w_i \left(\nabla \psi_i, \nabla \phi_j\right) = \omega^2 \left(\sum_{i=1}^n v_i \left(\phi_i, \phi_j\right) + \sum_{i=1}^m w_i \left(\psi_i, \phi_j\right) \right). \tag{11}$$

Finally, applying the linear finite element method with boundary conditions (2a), (2b) and the integration by parts to the difference equation between (1a) and (1b), we obtain

$$\begin{aligned} &\left(\sum_{i=1}^n (u_i - v_i) \nabla \phi_i, \nabla \psi_j \right) \\ &= \omega^2 \left(\sum_{i=1}^n u_i (\varepsilon \phi_i, \psi_j) + \sum_{i=1}^m w_i (\varepsilon \phi_i, \psi_j) - \sum_{i=1}^n v_i (\phi_i, \psi_j) - \sum_{i=1}^m w_i (\phi_i, \psi_j) \right). \end{aligned} \tag{12}$$

Hereafter, we define the stiffness matrices K, E, and mass matrices M_1, M_ε, F_1, F_ε, G_1 and G_ε as in Table 1. In addition, we set $\mathbf{u} = [u_1, \ldots, u_n]^\top$, $\mathbf{v} = [v_1, \ldots, v_n]^\top$, and $\mathbf{w} = [w_1, \ldots, w_m]^\top$. Then, the discretizations of (10), (11) and (12) give rise to a generalized eigenvalue problem (GEP)

$$\mathcal{A}\mathbf{z} = \lambda \mathcal{B}\mathbf{z} \tag{13a}$$

stiffness matrix for interior meshes	$K = [(\nabla\phi_i, \nabla\phi_j)] \succ 0 \in \mathbb{R}^{n\times n}$
stiffness matrix for interior/boundary meshes	$E = [(\nabla\phi_i, \nabla\psi_j)] \in \mathbb{R}^{n\times m}$
mass matrices for interior meshes with $\varepsilon = 1$ or $\varepsilon > 1$	$M_1 = [(\phi_i, \phi_j)] \succ 0 \in \mathbb{R}^{n\times n}$ $M_\varepsilon = [(\varepsilon\phi_i, \phi_j)] \succ 0 \in \mathbb{R}^{n\times n}$
mass matrices for interior/boundary meshes with $\varepsilon = 1$ or $\varepsilon > 1$	$F_1 = [(\phi_i, \psi_j)] \in \mathbb{R}^{n\times m}$ $F_\varepsilon = [(\varepsilon\phi_i, \psi_j)] \in \mathbb{R}^{n\times m}$
mass matrices for boundary meshes with $\varepsilon = 1$ or $\varepsilon > 1$	$G_1 = [(\psi_i, \psi_j)] \succ 0 \in \mathbb{R}^{m\times m}$ $G_\varepsilon = [(\varepsilon\psi_i, \psi_j)] \succ 0 \in \mathbb{R}^{m\times m}$

Table 1. Stiffness and mass matrices with $\varepsilon(x, y) > 1$ for $(x, y) \in \bar{D}$.

with $\lambda = \omega^2$,

$$\mathcal{A} = \begin{bmatrix} K & 0 & E \\ 0 & -K & E \\ E^\top & E^\top & 0 \end{bmatrix}, \quad \mathcal{B} = \begin{bmatrix} M_\varepsilon & 0 & F_\varepsilon \\ 0 & -M_1 & F_1 \\ F_\varepsilon^\top & F_1^\top & G_\varepsilon - G_1 \end{bmatrix}, \quad \mathbf{z} = \begin{bmatrix} \mathbf{u} \\ \mathbf{v} \\ \mathbf{w} \end{bmatrix}. \tag{13b}$$

For simplicity, we denote

$$G = G_\varepsilon - G_1, \quad M = M_\varepsilon - M_1, \quad F = F_\varepsilon - F_1, \tag{14a}$$

$$\widehat{M}_1 = M_1 - F_1 G^{-1} F^\top, \quad \widehat{M} = M - F G^{-1} F^\top, \quad \widehat{K} = K - E G^{-1} F^\top, \tag{14b}$$

and

$$\mathcal{S} = \begin{bmatrix} K & E \end{bmatrix}, \quad \mathcal{T}_1 = \begin{bmatrix} M_1 & F_1 \end{bmatrix}, \quad \mathcal{M} = \begin{bmatrix} M & F \\ F^\top & G \end{bmatrix}. \tag{14c}$$

Suppose that $\mathcal{M} \succ 0$ symmetric positive definite. Then it follows that $G \succ 0$, $M \succ 0$ and $\widehat{M} \succ 0$. The quadratic eigenvalue problem (QEP) is defined as

$$\mathcal{Q}(\lambda)\mathbf{x} \equiv \left(\lambda^2 A_2 + \lambda A_1 + A_0\right)\mathbf{x} = 0, \tag{15}$$

where A_2, A_1 and A_0 are all $n \times n$ symmetric matrices given by

$$\begin{aligned} A_2 &= M_1 + \widehat{M}_1 \widehat{M}^{-1} \widehat{M}_1^\top + F_1 G^{-1} F_1^\top \qquad (16a)\\ &= M_1 + \mathcal{T}_1 \mathcal{M}^{-1} \mathcal{T}_1^\top, \\ A_1 &= -K - \widehat{K}\widehat{M}^{-1}\widehat{M}_1^\top - \widehat{M}_1\widehat{M}^{-1}\widehat{K}^\top - E G^{-1} F_1^\top - F_1 G^{-1} E^\top \qquad (16b)\\ &= -K - \mathcal{S}\mathcal{M}^{-1}\mathcal{T}_1^\top - \mathcal{T}_1\mathcal{M}^{-1}\mathcal{S}^\top, \\ A_0 &= \widehat{K}\widehat{M}^{-1}\widehat{K}^\top + E G^{-1} E^\top \qquad (16c)\\ &= \mathcal{S}\mathcal{M}^{-1}\mathcal{S}^\top. \end{aligned}$$

It has been shown [13] that the GEP (13) can be reduced to the QEP as in (15) and (16) with $\mathbf{x} = \mathbf{u} - \mathbf{v}$ in which all nonphysical zero are removed.

Theorem 1 ([13]). *Let $\mathcal{L}(\lambda)$ and $\mathcal{Q}(\lambda)$ be matrix pencils defined as in (13) and (15), respectively. Then*

$$\sigma(\mathcal{L}(\lambda)) = \sigma(\mathcal{Q}(\lambda)) \cup \underbrace{\{0, \cdots, 0\}}_{m}.$$

Here, $\sigma(\cdot)$ denotes the spectrum of the associated matrix pencil.

Let $(\lambda, \mathbf{x})$ be an eigenpair of (15), then

$$\lambda^2(\mathbf{x}^* A_2 \mathbf{x}) + \lambda(\mathbf{x}^* A_1 \mathbf{x}) + (\mathbf{x}^* A_0 \mathbf{x}) = 0. \tag{17}$$

Suppose that A_1 is symmetric negative definite and $A_2, A_0 \succ 0$. We then obtain that

$$b \equiv -\mathbf{x}^* A_1 \mathbf{x} > 0, \quad a \equiv \mathbf{x}^* A_2 \mathbf{x} > 0, \quad c \equiv \mathbf{x}^* A_0 \mathbf{x} > 0$$

which imply that the roots of the quadratic equation (17) are

$$\lambda_+ = \frac{b + \sqrt{b^2 - 4ac}}{2a} > 0, \quad \lambda_- = \frac{2c}{b + \sqrt{b^2 - 4ac}} > 0 \tag{18}$$

provided that $b^2 - 4ac > 0$. Consequently, there are $2n$ positive eigenvalues of (15) and the associated eigenvectors are real.

Theorem 2. *Let*

$$W_0 = \begin{bmatrix} M & F \\ F^\top & G \end{bmatrix}^{-1/2} \begin{bmatrix} K \\ E^\top \end{bmatrix}, \quad W_1 = \begin{bmatrix} M & F \\ F^\top & G \end{bmatrix}^{-1/2} \begin{bmatrix} M_1 \\ F_1^\top \end{bmatrix}, \tag{19}$$

$$d_0 = \|W_0\|_2, \quad d_1 = \|W_1\|_2, \tag{20}$$

and

$$\begin{cases} \underline{a}_0 = \lambda_{\min}(A_0), & \bar{a}_0 = \lambda_{\max}(A_0) = d_0^2, \\ \underline{a}_2 = \lambda_{\min}(A_2), & \bar{a}_2 = \lambda_{\max}(A_2). \end{cases} \tag{21}$$

Suppose that

$$\underline{a}_1 = \lambda_{\min}(K) - 2d_0 d_1 > 0, \quad \bar{a}_1 = \lambda_{\max}(K) + 2d_0 d_1, \tag{22}$$

$$\delta = \lambda_{\min}(K)^2 - 4d_0(d_1 \lambda_{\min}(K) + d_0 \lambda_{\max}(M_1)) > 0. \tag{23}$$

Then there are n positive eigenvalues of (15) in the interval (r_*, r^*), where

$$r^* = \frac{2d_0^2}{\underline{a}_1 + \sqrt{\delta}}, \quad r_* = \frac{2\lambda_{\min}(A_0)}{\bar{a}_1 + \sqrt{\bar{a}_1 - 4\underline{a}_2 \underline{a}_0}} > 0. \tag{24}$$

Proof. By the definitions of W_0 and W_1, A_1 in (16b) can be expressed by

$$A_1 = -(K + W_0^\top W_1 + W_1^\top W_0). \tag{25}$$

Let $\mathbf{x}$ be the unit eigenvector of (15). Note that $\mathbf{x}$ is real. Eq. (25) implies that

$$\begin{aligned} b = -\mathbf{x}^\top A_1 \mathbf{x} &= \mathbf{x}^\top K \mathbf{x} + \mathbf{x}^\top W_0^\top W_1 \mathbf{x} + \mathbf{x}^\top W_1^\top W_0 \mathbf{x} \\ &\geq \lambda_{\min}(K) - 2d_0 d_1 = \underline{a}_1 > 0. \end{aligned}$$

Recall that $a = \mathbf{x}^\top A_2 \mathbf{x}$ and $c = \mathbf{x}^\top A_0 \mathbf{x}$. Then we have that

$$\begin{aligned} b^2 - 4ac &\geq (\lambda_{\min}(K) - 2d_0 d_1)^2 - 4d_0^2(\lambda_{\min}(M_1) + d_1^2) \\ &= \lambda_{\min}(K)^2 - 4d_0(d_1 \lambda_{\min}(K) + d_0 \lambda_{\max}(M_1)) = \delta > 0 \end{aligned}$$

and thus

$$\lambda_- = \frac{2c}{b + \sqrt{b^2 - 4ac}} \leq \frac{2d_0^2}{\underline{a}_1 + \sqrt{\delta}} = r^*.$$

On the other hand, we can see that

$$\begin{aligned} b = -\mathbf{x}^\top A_1 \mathbf{x} &\leq \lambda_{\max}(K) + 2d_0 d_1 = \bar{a}_1, \\ b^2 - 4ac &\leq \bar{a}_1^2 - 4\underline{a}_2 \underline{a}_0, \end{aligned}$$

which implies

$$\lambda_- = \frac{2c}{b + \sqrt{b^2 - 4ac}} \geq \frac{2\underline{a}_0}{\bar{a}_1 + \sqrt{\bar{a}_1^2 - 4\underline{a}_2 \underline{a}_0}} = r_*.$$

It follows from (18) that there are n smallest positive eigenvalues on (r_*, r^*). □

Remark 3. *By (16c), the value $\mathbf{x}^\top A_0 \mathbf{x}$ is dominated by $\mathbf{x}^\top \widehat{K} \widehat{M}^{-1} \widehat{K}^\top \mathbf{x}$ provided that $\lambda_{\min}(K) \equiv O(\kappa) \gg 1$. From (16a), $\mathbf{x}^\top A_2 \mathbf{x} \approx O(1)$ holds. If we can choose the coefficient $\varepsilon(x, y)$ in (1a) so that $\max|(M)_{ij}| \approx \max|(K)_{ij}|$, then from (24) it follows that*

$$\lambda_- \approx \frac{2O(\kappa)}{O(\kappa) + \sqrt{O(\kappa)^2 + O(\kappa)}} \approx O(1).$$

In other words, there are n positive eigenvalues of (1) which are densely distributed in the interval $(0, O(1))$. This motivates us to develop efficient numerical algorithms to compute all smallest clustering positive eigenvalues.

4. Non-equivalence low-rank deflation

In this section, we introduce the non-equivalence low-rank deflation [14] to locate the successive eigenpairs of the QEP in (15). Once the smallest positive eigenvalue is retrieved, we then transform it to infinity by the deflation scheme, while keeping all other eigenvalues unchanged. The next successive eigenvalue thus becomes the target positive eigenvalue of the new transformed problem, which is then repeatly solved by the proposed method.

Definition 4 ([14]). *Let* $(\Lambda_1, X_1) \in \mathbb{R}^{r\times r} \times \mathbb{R}^{n\times r}$ *with rank*$(X_1) = r$ *be a given pair.* (Λ_1, X_1) *is called an eigenmatrix pair of* $\mathcal{Q}(\lambda)$ *in* (15) *if it satisfies*

$$A_2X_1\Lambda_1^2 + A_1X_1\Lambda_1 + A_0X_1 = 0. \tag{26}$$

In particular, $(\mathrm{diag}(\infty, \cdots, \infty), X_1)$ *is called an* ∞*-eigenmatrix pair for* $\mathcal{Q}(\lambda)$ *if* $A_2X_1 = 0$.

Given an eigenmatrix pair $(\Lambda_1, X_1) \in \mathbb{R}^{r\times r} \times \mathbb{R}^{n\times r}(r \le n)$ of $\mathcal{Q}(\lambda)$ in (15) with Λ_1 being nonsingular, we define a new deflated QEP as

$$\mathcal{Q}_d(\lambda) := \lambda^2\widetilde{A}_2 + \lambda\widetilde{A}_1 + \widetilde{A}_0, \tag{27}$$

where

$$\widetilde{A}_2 := A_2 - A_2X_1\Theta_1X_1^\top A_2, \tag{28a}$$
$$\widetilde{A}_1 := A_1 + A_2X_1\Theta_1\Lambda_1^{-\top}X_1^\top A_0 + A_0X_1\Lambda_1^{-1}\Theta_1X_1^\top A_2, \tag{28b}$$
$$\widetilde{A}_0 := A_0 - A_0X_1\Lambda_1^{-1}\Theta_1\Lambda_1^{-\top}X_1^\top A_0, \tag{28c}$$

and

$$\Theta_1 := (X_1^\top A_2X_1)^{-1}. \tag{28d}$$

The nonequivalence deflation (28) allows us to transform $\mathcal{Q}(\lambda)$ into a new QEP $\mathcal{Q}_d(\lambda)$ with the same eigenvalues, except that the eigenvalues of Λ_1 are replaced by r infinities.

On the other hand, let $(\Lambda_2, X_2) \in \mathbb{R}^{s\times s} \times \mathbb{R}^{n\times s}$ be another eigenmatrix pair of $\mathcal{Q}(\lambda)$. Suppose that $\sigma(\Lambda_1) \cap \sigma(\Lambda_2) = \emptyset$. Then the following orthogonality relation holds [14]

$$X_2^\top A_0X_1 - \Lambda_2^\top(X_2^\top A_2X_1)\Lambda_1 = 0. \tag{29}$$

Using this orthogonality relation, we can see that (Λ_2, X_2) is also an eigenmatrix pair of $\mathcal{Q}_d(\lambda)$.

5. Jacobi-Davidson method for quadratic eigenvalue problems

In this section, we propose a quadratic Jacobi-Davidson (QJD) method [15, 29] combined with non-equivalence deflation scheme to solve the QEP (15). Suppose $\mathcal{V}_k$ is a k-dimensional subspace with an orthogonal unitary basis $\{\mathbf{v}_1, \mathbf{v}_2, \ldots, \mathbf{v}_k\}$. Let $V_k = [\mathbf{v}_1, \cdots, \mathbf{v}_k]$ and $(\theta_k, \mathbf{s}_k)$ be an eigenpair of $V_k^*\mathcal{Q}(\lambda)V_k\mathbf{s} = 0$ and $(\theta_k, \mathbf{u}_k \equiv V_k\mathbf{s}_k)$ be a Ritz pair of $\mathcal{Q}(\lambda)$ with $\|\mathbf{s}_k\|_2 = 1$. To expand the subspace $\mathcal{V}_k$ successively, the QJD method seaks an approximate solution for the correction equation:

$$\left(I - \frac{\mathbf{p}_k\mathbf{u}_k^*}{\mathbf{u}_k^*\mathbf{p}_k}\right)\mathcal{Q}(\theta_k)\left(I - \mathbf{u}_k\mathbf{u}_k^*\right)\mathbf{t} = -\mathbf{r}_k, \quad \mathbf{t}\perp\mathbf{u}_k, \tag{30}$$

where $\mathbf{r}_k = \mathcal{Q}(\theta_k)\mathbf{u}_k$ and $\mathbf{p}_k = (2\theta_kA_2 + A_1)\mathbf{u}_k$. This is a crucial step in the QJD method that may affect the overall performance significantly.

There are different schemes [15] for solving (30). Here, based on the coefficient matrices A_0, A_1, A_2 in (16), we adopt the scheme proposed in [15] to solve (30). Using the condition $\mathbf{t} \perp \mathbf{u}_k$, Eq. (30) can be rewritten as

$$\mathcal{Q}(\theta_k)\mathbf{t} = \frac{\mathbf{u}_k^* \mathcal{Q}(\theta_k)\mathbf{t}}{\mathbf{u}_k^* \mathbf{p}_k}\mathbf{p}_k - \mathbf{r}_k \equiv \eta_k \mathbf{p}_k - \mathbf{r}_k. \tag{31}$$

We can then solve the two linear systems

$$\mathcal{Q}(\theta_k)\mathbf{t}_1 = \mathbf{p}_k, \quad \mathcal{Q}(\theta_k)\mathbf{t}_2 = \mathbf{r}_k \tag{32a}$$

and compute the solution $\mathbf{t}$ of (31) as

$$\mathbf{t} = \eta_k \mathbf{t}_1 - \mathbf{t}_2 \quad \text{with} \quad \eta_k = \frac{\mathbf{u}_k^* \mathbf{t}_2}{\mathbf{u}_k^* \mathbf{t}_1}. \tag{32b}$$

Based on the above discussions, we summarize the quadratic Jacobi-Davidson method for the computation of the desired eigenvalue of the QEP (15) in Algorithm 1.

Algorithm 1 QJD method for $\mathcal{Q}(\lambda)\mathbf{x} \equiv (\lambda^2 A_2 + \lambda A_1 + A_0)\mathbf{x} = 0$.

Input: Coefficient matrices A_0, A_1, A_2 and an initial orthonormal matrix V.

Output: The desired eigenpair $(\lambda, \mathbf{x})$.

1: Compute $W_i = A_i V$ and $M_i = V^* W_i$ for $i = 0, 1, 2$.
2: **while** (the desired eigenpair is not convergent) **do**
3: Compute the eigenpairs $(\theta, \mathbf{s})$ of $(\theta^2 M_2 + \theta M_1 + M_0)\mathbf{s} = 0$.
4: Select the desired eigenpair $(\theta, \mathbf{s})$ with $\|\mathbf{s}\|_2 = 1$.
5: Compute $\mathbf{u} = V\mathbf{s}$, $\mathbf{p} = (2\theta A_2 + A_1)\mathbf{u}$, $\mathbf{r} = \mathcal{Q}(\theta)\mathbf{u}$.
6: Solve the correction vector $\mathbf{t}$ in (32).
7: Orthogonalize $\mathbf{t}$ against V; set $\mathbf{v} = \mathbf{t}/\|\mathbf{t}\|_2$.
8: Compute

$$\mathbf{w}_i = A_i \mathbf{v}, \quad M_i = \begin{bmatrix} M_i & V^* \mathbf{w}_i \\ \mathbf{v}^* W_i & \mathbf{v}^* \mathbf{w}_i \end{bmatrix}$$

for $i = 0, 1, 2$.
9: Expand $V = [V, \mathbf{v}]$ and $W_i = [W_i, \mathbf{w}_i]$ for $i = 0, 1, 2$.
10: **end while**
11: Set $\lambda = \theta$ and $\mathbf{x} = \mathbf{u}$.

Note that the solutions $\mathbf{t}_1$ and $\mathbf{t}_2$ in (32a) can be efficiently computed by the following way. Substituting A_2, A_1 and A_0 in (16) into (32a), Eq. (32a) can be represented as

$$\begin{aligned} \Big\{ \theta_k^2 M_1 - \theta_k K + \left(\theta_k \widehat{M}_1 - \widehat{K}\right) \widehat{M}^{-1} \left(\theta_k \widehat{M}_1^\top - \widehat{K}^\top\right) \\ + (\theta_k F_1 - E)\, G^{-1} \left(\theta_k F_1^\top - E^\top\right) \Big\} \mathbf{t} = \mathbf{b}, \end{aligned} \tag{33}$$

where $\mathbf{b} = \mathbf{p}_k$ or $\mathbf{b} = \mathbf{r}_k$. Let

$$\hat{\mathbf{t}} = \widehat{M}^{-1}\left(\theta_k \widehat{M}_1^\top - \widehat{K}^\top\right)\mathbf{t}, \quad \tilde{\mathbf{t}} = G^{-1}\left(\theta_k F_1^\top - E^\top\right)\mathbf{t},$$

which is equivalent to

$$\left(\widehat{K}^\top - \theta_k \widehat{M}_1^\top\right)\mathbf{t} + \widehat{M}\hat{\mathbf{t}} = 0, \quad \left(E^\top - \theta_k F_1^\top\right)\mathbf{t} + G\tilde{\mathbf{t}} = 0. \tag{34a}$$

Then (33) can be expressed by

$$\left(\theta_k K - \theta_k^2 M_1\right)\mathbf{t} + \left(\widehat{K} - \theta_k \widehat{M}_1\right)\hat{\mathbf{t}} + \left(E - \theta_k F_1\right)\tilde{\mathbf{t}} = -\mathbf{b}. \tag{34b}$$

Combining (34a) with (34b), the solution $\mathbf{t}$ in (33) can be solved from the augmented linear system

$$\begin{bmatrix} \widehat{M} & & \widehat{K}^\top - \theta_k \widehat{M}_1^\top \\ & G & E^\top - \theta_k F_1^\top \\ \widehat{K} - \theta_k \widehat{M}_1 & E - \theta_k F_1 & \theta_k K - \theta_k^2 M_1 \end{bmatrix} \begin{bmatrix} \hat{\mathbf{t}} \\ \tilde{\mathbf{t}} \\ \mathbf{t} \end{bmatrix} = \begin{bmatrix} 0 \\ 0 \\ -\mathbf{b} \end{bmatrix}. \tag{35}$$

5.1. Partial locking scheme

To compute successively all other desired eigenvalues, deflation [14, 16] or locking [15, 16, 17, 26] scheme is necessary. The Jacobi-Davidson method incorporated with locking scheme is capable of calculating the smallest positive eigenvalue first and then of computing all other desired eigenvalues successively by suitably choosing the orthonormal searching space $\mathrm{span}(V \equiv [V_c, V_0])$, where the columns of V_c form an orthonormal basis for the subspace generated by the convergent eigenvectors and V_0 is any matrix satisfying $V_0^\top V_0 = I$. Therefore, in each iteration of Algorithm 1, the convergent eigenvalues $\lambda_1, \ldots, \lambda_j$ will be included in the set of eigenvalues of the projective QEP $(\theta^2 M_2 + \theta M_1 + M_0)\mathbf{s} = 0$ in Line 3 of Algorithm 1. So, the target Ritz value θ in Line 4 of Algorithm 1 is chosen as $\theta \notin \{\lambda_1, \ldots, \lambda_j\}$.

Let $\{\lambda_1, \ldots, \lambda_m\}$ be the desired eigenvalues. If m is small, then the locking scheme can be applied to compute all desired eigenvalues successively. However, when m is large, locking all convergent eigenvectors in the searching subspace $\mathrm{span}(V)$ will reduce the efficiency significantly because it increases the costs of computing eigenpairs of $(\theta^2 M_2 + \theta M_1 + M_0)\mathbf{s} = 0$, the Ritz vectors $\mathbf{u}$, and the reorthogonalization of the correction vector $\mathbf{t}$ against V in Lines 1, 5 and 7, respectively, of Algorithm 1. In order to remedy this drawback, we propose a partial locking scheme with at most locking ℓ convergent eigenvectors in each iteration. Namely, for the computation of the $(j+1)$-th eigenpair $(\lambda_{j+1}, \mathbf{x}_{j+1})$ with $j+1 \le \ell$, all the convergent eigenvectors $\mathbf{x}_1, \ldots, \mathbf{x}_j$ are locked in V which means that the columns of V_c is an orthonormal basis of the subspace $\mathrm{span}\{\mathbf{x}_1, \ldots, \mathbf{x}_j\}$. If $j+1 > \ell$, then only the convergent eigenvectors $\mathbf{x}_{j+1-\ell}, \ldots, \mathbf{x}_j$ are locked. The algorithm is summarized in Algorithm 2.

Algorithm 2 Quadratic Jacobi-Davidson method with partial locking scheme.

Input: Coefficient matrices A_0, A_1, A_2, number p of desired eigenvalues, locking number ℓ ($\ell < p$) and an initial orthonormal matrix V.

Output: The desired eigenpair $(\lambda_j, \mathbf{x}_j)$ for $j = 1, \ldots, p$.

```
Set V_c = [ ];
for j = 1, ..., p do
    Use Algorithm 1 with initial matrix V to compute the desired eigenpair (λ_j, x_j);
    if j ≤ ℓ then
        Orthogonalize x_j against V_c; set V_c = [V_c, x_j/‖x_j‖_2];
    else
        Orthogonalize x_j against V_c(:, 2 : ℓ); set V_c = [V_c(:, 2 : ℓ), x_j/‖x_j‖_2];
    end if
    Find an initial matrix V_0 such that V_0^⊤ V_0 = I with V ≡ [V_c, V_0].
end for
```

5.2. Partial deflation scheme

In Section 4, an explicit nonequivalence low-rank deflation method is proposed to transform the convergent eigenvalues to the infinity, while all other eigenvalues remain unchanged. The next successive eigenvalue thus becomes the smallest positive one of the transformed problem. In this subsection, we will discuss how to efficiently apply QJD to solve the deflated QEP $\mathcal{Q}_d(\lambda)\mathbf{x} = 0$ in (27).

Let $Y_0 = A_0 X_1 \Lambda_1^{-1} \in \mathbb{R}^{n\times r}$ and $Y_2 = A_2 X_1 \in \mathbb{R}^{n\times r}$. Then the matrices $\widetilde{A}_2$, $\widetilde{A}_1$ and $\widetilde{A}_0$ defined in (28c) can be written as

$$\widetilde{A}_2 = A_2 - Y_2 \Theta_1 Y_2^\top, \tag{36a}$$

$$\widetilde{A}_1 = A_1 + Y_2 \Theta_1 Y_0^\top + Y_0 \Theta_1 Y_2^\top, \tag{36b}$$

$$\widetilde{A}_0 = A_0 - Y_0 \Theta_1 Y_0^\top. \tag{36c}$$

As stated in (32a), to solve the correction vector $\mathbf{t}_d$, we need to solve the linear system

$$\left(\theta_k^2 \widetilde{A}_2 + \theta_k \widetilde{A}_1 + \widetilde{A}_0\right) \mathbf{t} = \mathbf{b}. \tag{37}$$

In view of (36), (37) can be rewritten as

$$\left[\mathcal{Q}(\theta_k) - (\theta_k Y_2 - Y_0)\, \Theta_1 \left(\theta_k Y_2^\top - Y_0^\top\right)\right] \mathbf{t} = \mathbf{b}. \tag{38}$$

Denote

$$U = \theta_k Y_2 - Y_0.$$

Applying the Sherman-Morrison-Woodbury formula, the solution of (38) can be

computed as

$$\begin{aligned}\mathbf{t} &= \left\{\mathcal{Q}(\theta_k) - U\Theta_1 U^\top\right\}^{-1}\mathbf{b}\\ &= \mathcal{Q}(\theta_k)^{-1}\mathbf{b} + \mathcal{Q}(\theta_k)^{-1}U\left(I - \Theta_1 U^\top \mathcal{Q}(\theta_k)^{-1}U\right)^{-1}\Theta_1 U^\top \mathcal{Q}(\theta_k)^{-1}\mathbf{b}\\ &= \mathcal{Q}(\theta_k)^{-1}\mathbf{b} + \mathcal{Q}(\theta_k)^{-1}U\left(\Theta_1^{-1} - U^\top \mathcal{Q}(\theta_k)^{-1}U\right)^{-1}U^\top \mathcal{Q}(\theta_k)^{-1}\mathbf{b}.\end{aligned}$$

In other words, in each iteration, we need to solve the linear systems

$$\mathcal{Q}(\theta_k)Z = \begin{bmatrix}\tilde{\mathbf{p}}_k & \tilde{\mathbf{r}}_k & U\end{bmatrix}, \tag{39a}$$

where $\tilde{\mathbf{r}}_k = \mathcal{Q}_d(\theta_k)\tilde{\mathbf{u}}_k$ and $\tilde{\mathbf{p}}_k = (2\theta_k\widetilde{A}_2 + \widetilde{A}_1)\tilde{\mathbf{u}}_k$, and compute the correction vector $\mathbf{t}_d$ as

$$\mathbf{t}_d = \eta_k\tilde{\mathbf{t}}_1 - \tilde{\mathbf{t}}_2 \quad \text{with} \quad \eta_k = \frac{\tilde{\mathbf{u}}_k^*\tilde{\mathbf{t}}_2}{\tilde{\mathbf{u}}_k^*\tilde{\mathbf{t}}_1} \tag{39b}$$

where

$$\tilde{\mathbf{t}}_1 = Z(:,1) + Z(:,3:r+2)(\Theta_1^{-1} - U^\top Z(:,3:r+2))^{-1}U^\top Z(:,1), \tag{39c}$$
$$\tilde{\mathbf{t}}_2 = Z(:,2) + Z(:,3:r+2)(\Theta_1^{-1} - U^\top Z(:,3:r+2))^{-1}U^\top Z(:,2). \tag{39d}$$

From above, we can see that the computational cost of solving $\mathcal{Q}_d(\lambda)\mathbf{x} = 0$ by QJD will be increasing as r increases. In order to reduce the computational cost, similar to the concept of partial locking scheme, we propose a partial deflation scheme with at most deflating ℓ convergent eigenvectors in each iteration. That is, for computing the $(j+1)$-th eigenpair $(\lambda_{j+1}, \mathbf{x}_{j+1})$ with $j+1 \le \ell$, all the convergent eigenvectors $\mathbf{x}_1, \ldots, \mathbf{x}_j$ are deflated. If $j+1 > \ell$, then only the convergent eigenvectors $\mathbf{x}_{j+1-\ell}, \ldots, \mathbf{x}_j$ are deflated. We summarize the steps in Algorithm 3.

6. Numerical results

In what follows, we will compare the efficiency of Algorithm 2 with $\ell = 20$ and Algorithm 3 with $\ell = 10$ for computing desired positive real transmission eigenvalues $\lambda_i > 0$, $i = 1, \ldots, p$, on four different domains [25] as shown in Figure 1. The meshes for these domains are constructed by triangular meshes. The associated matrix dimensions n and m of matrices in Table 1 are listed in Table 2. The distributions of $\{\lambda_1, \ldots, \lambda_p\}$ with $\varepsilon(x, y) = 50, 100, 500, 1000$ and matrix dimensions n and m in Table 2 are shown in Figures 1(e), 1(f), 1(g) and 1(h), respectively. All the eigenvalues almost have an uniform distribution.

All computations for numerical test examples are carried out in MATLAB 2015b. The linear system in (35) is solved by Gaussian elimination (i.e., left matrix divide in MATLAB). Tic and toc functions are used to measure elapsed time in second. For the hardware configuration, we use an HP server equipped with the RedHat Linux operating system, two Intel Quad-Core Xeon E5-2643 3.33 GHz CPUs and 96 GB of main memory.

Algorithm 3 Quadratic Jacobi-Davidson method with partial deflation scheme.

Input: Coefficient matrices A_0, A_1, A_2, number p of desired eigenvalues, number ℓ ($\ell < p$) of deflation and an initial orthonormal matrix V.

Output: The desired eigenpair $(\lambda_j, \mathbf{x}_j)$ for $j = 1, \ldots, p$.

1: Set $X_1 = [\,]$, $Y_0 = [\,]$, $Y_2 = [\,]$ and $\Theta = [\,]$;
2: **for** $j = 1, \ldots, p$ **do**
3: Use Algorithm 1 with the initial matrix V and solve the correction vector $\mathbf{t}_d$ by (39) to compute the first desired eigenpair $(\lambda_j, \mathbf{x}_j)$ of $\mathcal{Q}_d(\lambda)\mathbf{x} = 0$;
4: Compute $\mathbf{y}_0 = \lambda_j^{-1} A_0 \mathbf{x}_j$ and $\mathbf{y}_2 = A_2 \mathbf{x}_j$;
5: **if** $j \le \ell$ **then**
6: Set $\Theta = \begin{bmatrix} \Theta & X_1^\top \mathbf{y}_2 \\ \mathbf{x}_j^\top Y_2 & \mathbf{x}_j^\top \mathbf{y}_2 \end{bmatrix}$, $\Theta_1 = \Theta^{-1}$, $X_1 = [X_1, \mathbf{x}_j]$, $Y_0 = [Y_0, \mathbf{y}_0]$ and $Y_2 = [Y_2, \mathbf{y}_2]$;
7: **else**
8: Set $\Theta = \begin{bmatrix} \Theta(2:\ell, 2:\ell) & X_1(:, 2:\ell)^\top \mathbf{y}_2 \\ \mathbf{x}_j^\top Y_2(:, 2:\ell) & \mathbf{x}_j^\top \mathbf{y}_2 \end{bmatrix}$ and $\Theta_1 = \Theta^{-1}$;
9: Set $X_1 = [X_1(:, 2:\ell), \mathbf{x}_j]$, $Y_0 = [Y_0(:, 2:\ell), \mathbf{y}_0]$ and $Y_2 = [Y_2(:, 2:\ell), \mathbf{y}_2]$;
10: **end if**
11: Update the initial matrix V.
12: **end for**

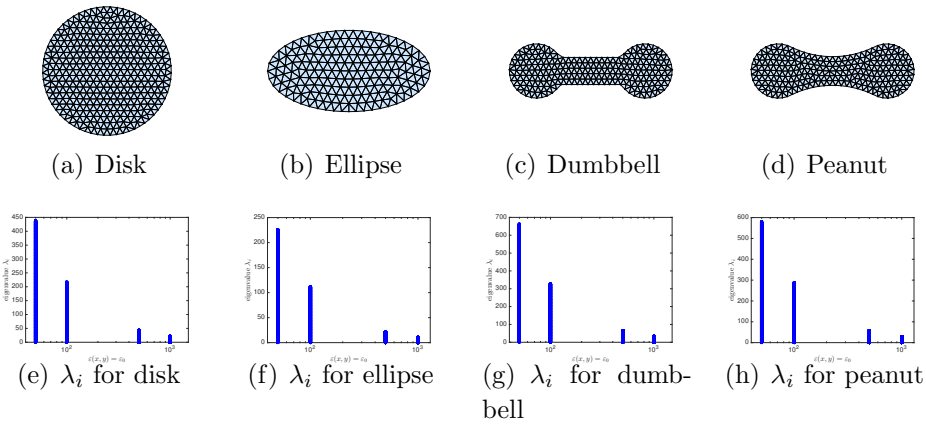

(a) Disk (b) Ellipse (c) Dumbbell (d) Peanut

(e) λ_i for disk (f) λ_i for ellipse (g) λ_i for dumbbell (h) λ_i for peanut

Figure 1. Model domains and the associated distributions of the 5000 positive target eigenvalues for $\varepsilon(x, y) = 50, 100, 500, 1000$.

Table 2. The matrix dimension n, m ($K \in \mathbb{R}^{n\times n}$, $E \in \mathbb{R}^{n\times m}$) of the matrices for the benchmark problems. Here the mesh size $h \approx 0.04$.

Domain	disk	ellipse	dumbbell	peanut
(n, m)	(124631, 1150)	(71546, 976)	(149051, 1871)	(168548, 1492)

Table 3. The first and pth eigenvalues λ_1 and λ_p computed by Algorithm 3 and the associated $(e_1(\varepsilon_0), e_p(\varepsilon_0))$ defined in (40), where $p = 5000$ and $\varepsilon_0 = 5000$.

Domain	disk	ellipse
$(e_1(\varepsilon_0), e_p(\varepsilon_0))$	$(0.00290, 4.25)$	$(1.837 \times 10^{-3}, 2.129)$
(λ_1, λ_p)	$(0.00294, 4.28)$	$(2.087 \times 10^{-3}, 2.210)$
(r_1, r_p)	$(0.014, 0.007)$	$(0.119, 0.037)$
Domain	dumbbell	peanut
$(e_1(\varepsilon_0), e_p(\varepsilon_0))$	$(0.0113, 6.42)$	$(6.392 \times 10^{-3}, 5.621)$
(λ_1, λ_p)	$(0.0114, 6.49)$	$(6.440 \times 10^{-3}, 5.673)$
(r_1, r_p)	$(0.009, 0.011)$	$(0.007, 0.009)$

6.1. Numerical validation for the clustering eigenvalues

In this section, we shall numerically validate that the TEP has densely distributed eigenvalues in the interval $(0, O(1))$ if the coefficient $\varepsilon(x, y)$ in (1a) is sufficient large as shown in Remark 3. Furthermore, we shall demonstrate that each eigencurve vs $\varepsilon(x, y)$ can be numerically approximated by a nonlinear function.

In order to observe the variety of the distribution of the eigenvalues with various coefficients $\varepsilon(x, y)$, we compute the fifty smallest positive real eigenvalues for each given constant $\varepsilon(x, y) = \varepsilon_0$ and show the computed eigenvalues in Figures 2(a), 2(c), 2(e) and 2(g). From these results, we see that the distributions of these fifty eigenvalues are clustered to the interval (0.2,1) as ε_0 approaches to 10^3.

On the other hand, these results also show that each eigencurve $\lambda_i(\varepsilon_0)$ can be approximated by a nonlinear function

$$\lambda_i(\varepsilon_0) \approx e_i(\varepsilon_0) \equiv b_i \times \varepsilon_0^{-a_i} \tag{40}$$

with constant a_i and b_i for $i = 1, \ldots, 50$. We show the nonlinear functions $e_1(\varepsilon)$ and $e_{50}(\varepsilon)$ in Figures 2(a), 2(c), 2(e) and 2(g) with red lines. These approximations can be extended to other eigencurves. Using the eigenvalues shown in Figures 1(e), 1(f), 1(g) and 1(h), we get the coefficients a_i and b_i for $i = 1, \ldots, 5000$ as shown in Figures 2(b), 2(d), 2(f) and 2(h), respectively. The approximation in (40) can be used to estimate the eigenvalues for a given ε_0. In Table 3, we demonstrate the computed eigenvalues λ_1 and λ_p by Algorithm 3 and $(e_1(\varepsilon_0), e_p(\varepsilon_0))$ in (40) for $\varepsilon_0 = 5000$ and $p = 5000$ with the domains in Figure 1. The results show that the relative errors $r_i \equiv |\lambda_i - e_i|/|\lambda_i|$ can be achieved about 0.01 for $i = 1$ and p.

Furthermore, the curves of the coefficients a_i and b_i for $i = 1, \ldots, 5000$ in Figures 2(b), 2(d), 2(f) and 2(h) can be approximated by a linear function

$$a_i \approx \ell_a(i) \equiv \alpha_1 \times i + \alpha_0 \tag{41a}$$

and a nonlinear function

$$b_i \approx e_b(i) \equiv \beta_0 \times i^{\beta_1} \times 10^{\beta_2 (\log_{10}(i))^2}, \tag{41b}$$

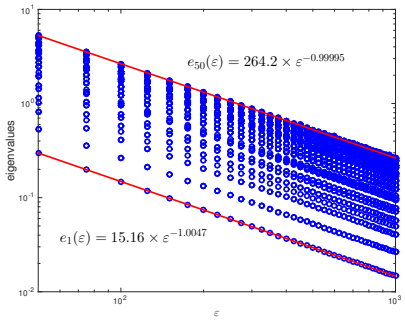

(a) Eigenvalues for disk

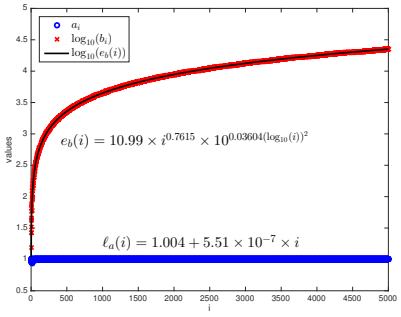

(b) Coefficients a_i and b_i for disk

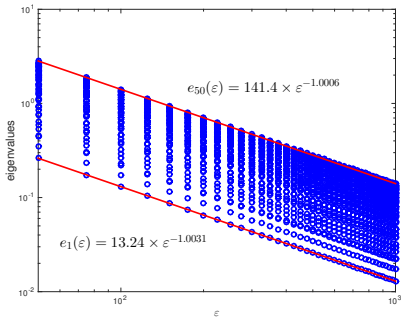

(c) Eigenvalues for ellipse

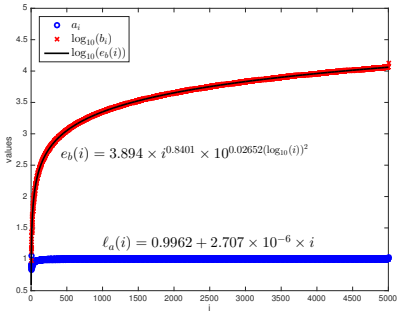

(d) Coefficients a_i and b_i for ellipse

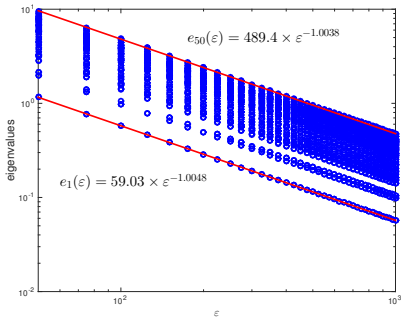

(e) Eigenvalues for dumbbell

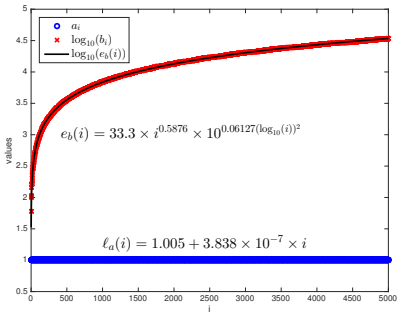

(f) Coefficients a_i and b_i for dumbbell

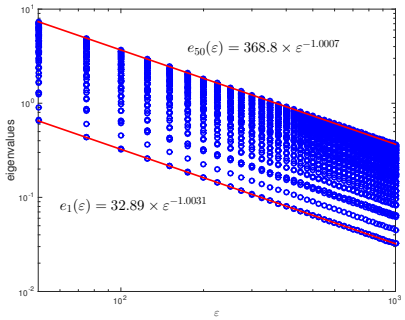

(g) Eigenvalues for peanut

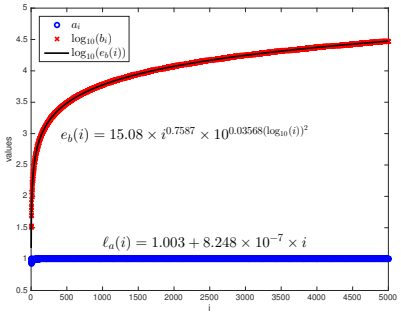

(h) Coefficients a_i and b_i for peanut

Figure 2. Eigenvalues with various $\varepsilon(x, y)$ and the coefficients a_i and b_i in the nonlinear functions.

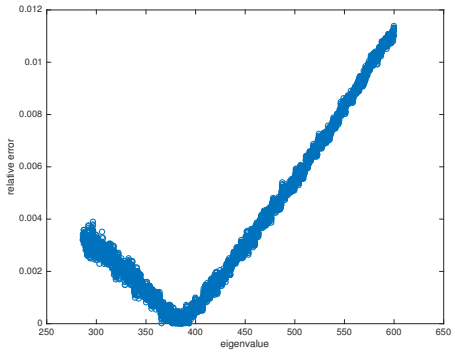

Figure 3. Relative errors of approximations $e(100, i)$ for $i = 5001, \ldots, 10105$.

respectively, as shown in the associated figures. Substituting (41) into (40), we can see that the positive eigencurve $\lambda_i(\varepsilon)$ can be approximated by

$$\lambda_i(\varepsilon) \approx e(\varepsilon, i) \equiv \beta_0 \times i^{\beta_1} \times 10^{\beta_2(\log_{10}(i))^2} \times \varepsilon^{-(\alpha_1 \times i + \alpha_0)}.$$

Comparing with the eigenvalues $\lambda_i(100)$, for $i = 5001, \ldots, 10105$, of the TEP with peanut domain as shown in Figure 6(b), the relative errors $|\lambda_i(100) - e(100, i)|/\lambda_i(100)$ for $i = 5001, \ldots, 10105$ range from 5×10^{-7} to 0.012 as shown in Figure 3. This demonstrates that $e(\varepsilon, i)$ is a good approximation for the eigencurve.

6.2. Numerical comparisons of locking and deflation schemes

Let μ_k denote the number of the target eigenvalues which are computed by QJD in Algorithm 1 with k iterations. If $k \geq 16$, then we define $\mu_{16} := \sum_{k \geq 16} \mu_k$. On the other hand, we denote T_l and T_d the average of the CPU times in seconds for computing p target positive smallest eigenvalues by Algorithms 2 and 3, respectively.

In Figure 4, we show the percentage μ_k/p for $k = 0, 1, \ldots, 16$ with $\varepsilon_0 = 50, 100, 500, 1000$. The results indicate that the iteration numbers k of Algorithm 3 with deflation scheme are concentrated at $k = 4, 5, 6$ for each ε_0. However, the iteration number k of Algorithm 2 with locking scheme depends on ε_0. The iteration number is concentrated at $4, 5, 6$ only when ε_0 is large enough as shown in Figures 4(c) and 4(d). Figures 4(a) and 4(b) show that, in average, locking schemes need more and more iterations to compute the target eigenpair as ε_0 becomes smaller. When the convergent eigenvectors are locked into the searching subspace span$\{V\}$, the small size QEP $(\theta^2 M_2 + \theta M_1 + M_0)\mathbf{s} = 0$ in Line 3 at Algorithm 1 will produce dummy Ritz pairs. The convergence of the locking scheme can be affected by such dummy Ritz pairs when the distribution of the eigenvalues is not clustered, for example, $\varepsilon_0 = 50, 100$. In the deflation scheme, there is no dummy Ritz pairs created by the convergent eigenvectors. This is one of the reasons that, in average, the iteration number for the deflation scheme is less than that for the locking scheme when ε_0 ranges from 50 to 500.

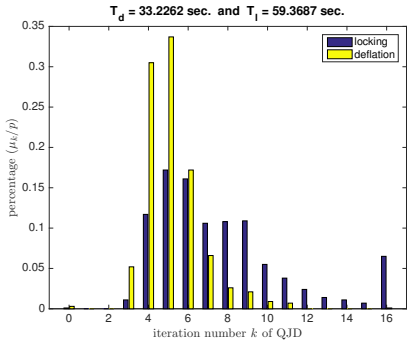

(a) Ellipse with $\varepsilon_0 = 50$ and $p = 1000$

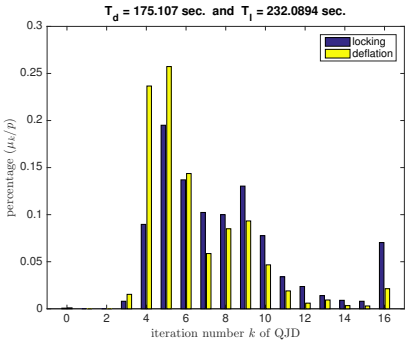

(b) Peanut with $\varepsilon_0 = 100$ and $p = 3000$

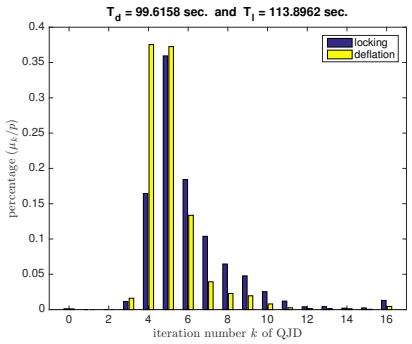

(c) Dumbbell with $\varepsilon_0 = 500$ and $p = 5000$

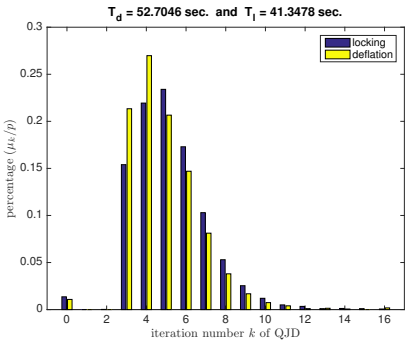

(d) Disk with $\varepsilon_0 = 1000$ and $p = 5000$

Figure 4. Percentages $\frac{\mu_k}{p}$ for the locking scheme and the deflation scheme with various ε_0.

From Section 5, we can see that the computational cost of the deflation scheme is more than that of the locking scheme in each iteration. As shown in Figures 4(a), 4(b) and 4(c), due to the fact that the total iterations of deflation scheme are less than that of locking scheme for $\varepsilon_0 = 50$, 100 and 500, the average time T_d is less than T_l. For $\varepsilon_0 = 1000$, both the iteration numbers of the locking and the deflation schemes are concentrated at $3, 4, 5, 6$. This leads to $T_d > T_l$ as shown in Figure 4(d).

In order to demonstrate that less iterations are needed for solving the TEP using the deflation scheme, we compute the first 5000 eigenpairs of the TEP with domains in Figure 1 using Algorithm 3. The percentages $\frac{\mu_k}{p}$ with $\varepsilon_0 = 50, 100, 500, 1000$ are shown in Figure 5. The numerical results demonstrate that only when $\varepsilon_0 = 50$, more iterations of the QJD are needed to compute the target eigenvalues. The most iterations of the QJD are concentrated at $3, 4, 5, 6$ for other ε_0's.

Remark 5. (i). *Theorem 2 indicates that the QEP (15) has a set of densely distributed positive eigenvalues when $\varepsilon(x, y)$ is chosen sufficiently large. From Figure 4, we can see that, in average, the CPU time for computing one eigenpair of the TEP by Algorithm 3 ranges from* 33 *seconds to* 175 *seconds with associated matrix dimensions being* 71546 *and* 168548*, respectively. This result shows that densely distributed positive eigenvalues*

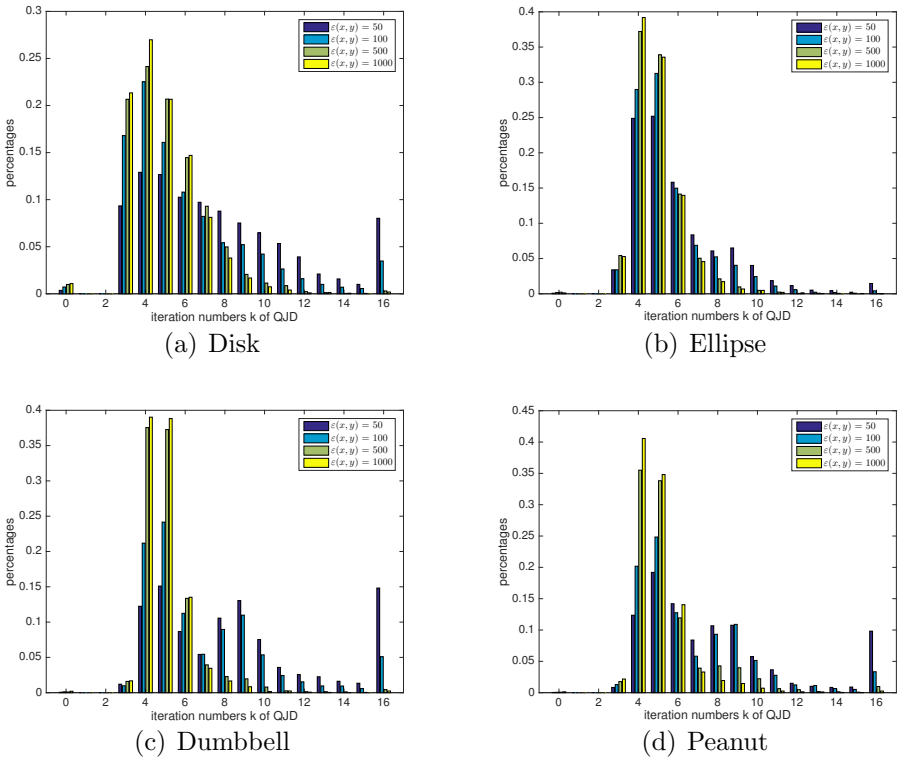

(a) Disk (b) Ellipse

(c) Dumbbell (d) Peanut

Figure 5. Percentage $\frac{\mu_k}{p}$ for the deflation scheme with various ε_0.

of the TEP can be efficiently computed by Algorithm 3.

(ii). *When $\varepsilon(x, y)$ is close to* 1*, the desired positive eigenvalues of* (15) *are surrounded by complex ones. Due to this fact, these positive eigenvalues are hard to be computed by the QJD. Thus, to compute them more efficiently, several secant-type iteration methods were proposed [13, 18, 25]. In each iteration of the secant-type method, the approximated eigenvalues can be guaranteed to be real. But, for computing the densely distributed positive eigenvalues (in the case where ε is large), secant-type iteration methods need more and more iterations than that of QJD. In other words, QJD outperforms secant-type methods for large $\varepsilon(x, y)$.*

6.3. Computing the eigenvalues in the given interval

In Subsection 6.2, we have demonstrated that Algorithms 2 and 3 can be applied to compute a lot of the target eigenpairs sequentially. Even each target eigenvalue can be efficiently computed by the proposed methods, the total CPU time becomes very large when the number of target eigenvalues is huge. In order to reduce the total CPU time, we slightly modify Algorithm 3 so that it can be applied to compute the eigenvalues in a given interval. We name it as Mod. Alg. 3. Therefore, the target eigenvalues can be computed by Mod. Alg. 3 in parallel with a given different interval. In Figure 6, we show the results of the peanut domain with $\varepsilon_0 = 100$ and the given intervals $(10i, 10(i + 1)]$

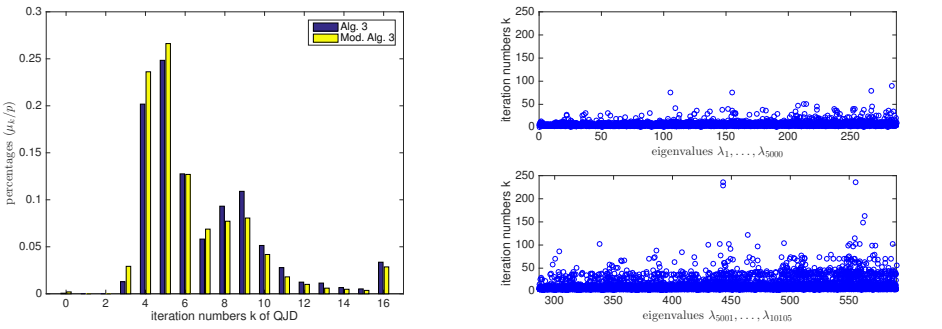

(a) Percentage $\frac{\mu_k}{p}$ for $\lambda_1, \ldots, \lambda_{5000}$

(b) Iteration numbers k of QJD for computing λ_i, $i = 1, \ldots, 10105$

Figure 6. Peanut with $\varepsilon(x, y) = 100$.

for $i = 0, 1, \ldots, 59$. In other words, we apply Mod. Alg. 3 to compute all eigenvalues in the interval $(0, 600]$.

Comparing the percentages $\frac{\mu_k}{5000}$ in computing $\lambda_1, \ldots, \lambda_{5000}$ with Algorithm 3 and Mod. Alg. 3, the results of Figure 6(a) show that the percentages $\frac{\mu_3+\cdots+\mu_7}{5000}$ for Algorithm 3 and Mod. Alg. 3 are equal to 0.6488 and 0.7274, respectively. This indicates that, in average, the convergence of Mod. Alg. 3 is better than that of Algorithm 3. On the other hand, in Figure 6(b), we demonstrate the iteration steps of the QJD in Mod. Alg. 3 for computing each eigenvalue. These numerical results show that the larger the target eigenvalue, the more iterations of the QJD.

7. Conclusion

In this paper, we propose a numerical algorithm to compute positive interior transmission eigenvalues (densely distributed) for the two-dimensional acoustic scattering problem that is derived from Maxwell's equations with the TM mode in non-reciprocal and non-chiral media having material parameters $\varepsilon(x, y)$, γ, and $\varepsilon(x, y) = \tilde{\varepsilon}(x, y) + \gamma^2$. The associated discretized eigenvalue problem is related to a generalized eigenvalue problem which can be reduced to a QEP by deflating all nonphysical zeros. Our numerical simulations indicate that half of the positive eigenvalues of the QEP are densely distributed in some interval near the origin. The QJD method with partial locking technique is proposed to compute such densely distributed eigenvalues of the QEP. In order to accelerate convergence, we also develop a so-called non-equivalence deflation technique combined with QJD to deflate the part of computed eigenvalues to infinity while keeping the other eigenvalues unchanged. Numerical results demonstrate that the deflation technique makes the convergence efficiently. The locking technique outperforms the deflation technique in timing only when eigenvalues of the QEP are typically clustering together in our model. Numerical results also illustrate that the eigenvalue curves can be approximated by the nonlinear functions so that we can apply

these nonlinear functions to estimate the eigenvalues for a given constant $\varepsilon(x, y)$.

Acknowledgments

The authors are grateful to the anonymous referees for their useful comments and suggestions. Li is supported in parts by the NSFC 11471074 and 91330109. Huang was partially supported by the Ministry of Science and Technology (MOST) 105-2115-M-003-009-MY3, National Center of Theoretical Sciences (NCTS) in Taiwan. Lin was partially supported by MOST, NCTS and ST Yau Center in Taiwan. Wang was partially supported by MOST 105-2115-M-002-014-MY3.

References

[1] F. Cakoni and D. Colton. *Qualitative methods in inverse scattering theory: An introduction*. Springer Science & Business Media, 2005.

[2] F. Cakoni, D. Colton, and H. Haddar. On the determination of Dirichlet or transmission eigenvalues from far field data. *C. R. Math. Acad. Sci. Pairs*, 348(7-8):379–383, 2010.

[3] F. Cakoni, D. Colton, P. Monk, and J. Sun. The inverse electromagnetic scattering problem for anisotropic media. *Inv. Prob.*, 26(7):074004, 2010.

[4] F. Cakoni, D. Gintides, and H. Haddar. The existence of an infinite discrete set of transmission eigenvalues. *SIAM J. Math. Anal.*, 42(1):237–255, 2010.

[5] F. Cakoni and H. Haddar. On the existence of transmission eigenvalues in an inhomogeneous medium. *Appl. Anal.*, 88(4):475–493, 2009.

[6] F. Cakoni and H. Haddar. Transmission eigenvalues in inverse scattering theory. In G. Uhlmann, editor, *Inverse Problems and Applications: Inside Out II*, volume 60 of *Math. Sci. Res. Inst. Publ.*, pages 527–578. Cambridge University Press, Cambridge, 2012.

[7] D. Colton and A. Kirsch. A simple method for solving inverse scattering problems in the resonance region. *Inv. Prob.*, 12(4):383, 1996.

[8] D. Colton and R. Kress. *Inverse Acoustic and Electromagnetic Scattering Theory*, volume 93 of *Applied Mathematical Sciences*. Springer, New York, 3rd edition, 2013.

[9] D. Colton and P. Monk. A novel method for solving the inverse scattering problem for time-harmonic acoustic waves in the resonance region. *SIAM J. Appl. Math.*, 45:1039–53, 1985.

[10] D. Colton, P. Monk, and J. Sun. Analytical and computational methods for transmission eigenvalues. *Inv. Prob.*, 26:045011, 2010.

[11] D. Colton, L. Päivärinta, and J. Sylvester. The interior transmission problem. *Inv. Prob. Imaging*, 1(1):13–28, 2007.

[12] G. C. Hsiao, F. Liu, J. Sun, and L. Xu. A coupled BEM and FEM for the interior transmission problem in acoustics. *J. Comput. Appl. Math.*, 235:5213–5221, 2011.

[13] T.-M. Huang, W.-Q. Huang, and W.-W. Lin. A robust numerical algorithm for computing Maxwell's transmission eigenvalue problems. *SIAM J. Sci. Comput.*, 37:A2403–A2423, 2015.

[14] T.-M. Huang and W.-W. Lin. A novel deflation technique for solving quadratic eigenvalue problems. *Bulletin of the Institute of Mathematics, Academia Sinica (New Series)*, 9:57–84, 2014.

[15] T.-M. Huang, W. Wang, and C.-T. Lee. An efficiency study of polynomial eigenvalue problem solvers for quantum dot simulations. *Taiwanese J. Math.*, 14:999–1021, 2010.

[16] T.-M. Hwang, W.-W. Lin, J.-L. Liu, and W. Wang. Jacobi-Davidson methods for cubic eigenvalue problems. *Numer. Linear Algebra Appl.*, 12:605–624, 2005.

[17] T.-M. Hwang, W.-W. Lin, W.-C. Wang, and W. Wang. Numerical simulation of three dimensional pyramid quantum dot. *J. Comput. Phys.*, 196:208–232, 2004.

[18] X. Ji, J. Sun, and T. Turner. Algorithm 922: A mixed finite element method for Helmholtz transmission eigenvalues. *ACM Trans. Math. Software*, 38:29, 2012.

[19] X. Ji, J. Sun, and H. Xie. A multigrid method for Helmholtz transmission eigenvalue problems. *J. Sci. Comput.*, 60(2):276–294, 2014.

[20] A. Kirsch. On the existence of transmission eigenvalues. *Inv. Prob. Imaging*, 3(2):155–172, 2009.

[21] A. Kirsch and N. Grinberg. *The factorization method for inverse problems.* Number 36. Oxford University Press, 2008.

[22] A. Kleefeld. A numerical method to compute interior transmission eigenvalues. *Inv. Prob.*, 29(10):104012, 2013.

[23] A. Kleefeld. A numerical method to compute electromagnetic interior transmission eigenvalues. In *12th international conference on mathematical and numerical aspects of wave propagation.* Karlsruhe Institute of Technology, 20-24 July 2015.

[24] A. Kleefeld. *Numerical methods for acoustic and electromagnetic scattering: Transmission boundary-value problems, interior transmission eigenvalues, and the factorization method.* Habilitation Thesis, May 2015.

[25] T. Li, W.-Q. Huang, W.-W. Lin, and J. Liu. On spectral analysis and a novel algorithm for transmission eigenvalue problems. *J. Sci. Comput.*, 64(1):83–108, 2015.

[26] K. Meerbergen. Locking and restarting quadratic eigenvalue solvers. *SIAM J. Sci. Comput.*, 22:1814–1839, 2001.

[27] L. Päivärinta and J. Sylvester. Transmission eigenvalues. *SIAM J. Math. Anal.*, 40(2):738–753, 2008.

[28] A. Serdyukov, I. Semchenko, S. Tretyakov, and A. Sihvola. *Electromagnetics of Bi-anisotropic Materials: Theory and Applications.* Gordon and Breach Science, 2001.

[29] G. L. G. Sleijpen, A. G. L. Booten, D. R. Fokkema, and H. A. van der Vorst. Jacobi-Davidson type methods for generalized eigenproblems and polynomial eigenproblems. *BIT*, 36:595–633, 1996.

[30] J. Sun. Estimation of transmission eigenvalues and the index of refraction from cauchy data. *Inv. Prob.*, 27(1):015009, 2010.

[31] J. Sun. Iterative methods for transmission eigenvalues. *SIAM J. Numer. Anal.*, 49(5):1860–1874, 2011.

[32] J. Sun. An eigenvalue method using multiple frequency data for inverse scattering problems. *Inv. Prob.*, 28:025012, 2012.

[33] J. Sun and L. Xu. Computation of Maxwell's transmission eigenvalues and its applications in inverse medium problems. *Inv. Prob.*, 29:104013, 2013.

[34] J. Sun and A. Zhou. *Finite Element Methods for Eigenvalue Problems.* Boca Raton: CRC Press, 2017.

[35] W. S. Weiglhofer and A. Lakhtakia. *Introduction to Complex Mediums for Optics and Electromagnetics.* SPIE, Washington, DC, 2003.